ISSN (Online) 2456-1290

International Journal of Engineering Research in Mechanical and Civil Engineering (IJERMCE)

Vol 10, Issue 10, October 2023

A New Stress Instability Workability Criterion for Internal Ductile Failure in Steel Cold Heading Process

[1] Amar Sabih, [2] James Nemes

[1] Concordia University-McGill University
[2] Penn State Great Valley University
Corresponding Author Email: [1] amar.sabih@concordia.ca, amar.sabih@mcgill.ca, [2] jan16@psu.edu

***Abstract*— The occurrence of internal ductile failure within the Adiabatic Shear Band (ASB) in cold-headed products presents a significant barrier in the fast-expanding cold-heading (CH) industry. The presence of internal ductile failure in cold-headed products may lead to catastrophic fracture under tensile loads despite the ductile nature of the material causing expensive industrial recalls. Therefore, this paper presents a new workability criterion that uses the ratio between the equivalent stress at instability and failure as an indicator to accurately reveal the locus of initiation of internal ductile failures.**

The concept of the instability criterion is to use the stress ratio at failure as a weighting function to indicate the initiation of ductile failure inside the ASBs.

This paper presents a comprehensive experimental, metallurgical, and finite element simulation study to calculate the material constants used in this criterion.

***Index Terms*— Adiabatic Shear Band, Cold-heading, Ductile Failure, Stress Instability, Workability Criterion.**

I. INTRODUCTION

The cold-heading (CH) process is a complicated process where the cold-headed product quality relies on the complex interplay of material and process parameters. Unfortunately, the design of cold-headed products is based on many rules of thumb developed over many decades using the accumulated information of the experimental and trial and error expertise. Nowadays, applying these rules in higher strains and strain rates of CH processes proved that they are not able to provide suitable CH process designs to produce defect-free products.

Sabih and Nemes [1] showed in their experimental and FE analysis study that increasing the CH strain rates and strains lead to internal failure caused by the adiabatic shear band (ASB) phenomenon. The outcomes of this work confirmed that ASBs develop through complicated stages leading to a sudden drop in flow stress triggered by the stress instability phenomenon.

Clifton [2], Bai [3], Merzer [4], and Wright and Batra [5] among others, observed that with increasing strain, stress reached a maximum value and then began a slow decrease followed by the initiation of a rapid collapse. This critical stage is triggered by the stress instability phenomenon that leads to localization and eventually to ductile failure. Therefore, this can be considered an important approach in setting the workability limits for ductile failure caused by the ASB phenomenon because the instability condition is an important stage for the following fast failure.

The main objective of this work is to present a new workability criterion based on the onset of instability phenomenon within the ASBs. to characterize the development stages of ASBs as well as to investigate the role of different processes and material parameters on the ASB development stages in cold-headed parts.

In the following sections, details about the ASB types, stages and the failure associated with these bands will be introduced. This introduction is followed by details about the experimental and finite element (FE) modelling procedure used in studying the ASB phenomenon. After presenting the experimental and FE results, the last part of this paper focuses on discussing these findings and introducing the final conclusion.

1.1 Adiabatic shear band (ASB) phenomenon

Meyers and Wittman [6] stated that the adiabatic shear band (ASB) term is reserved for shear bands that develop in strain rates higher than 102 s^{-1}. The term “adiabatic” is used since heat loss during deformation is small relative to heat generation. Klepaczko and Rezaig [7] reported in their studies of the ASB phenomenon that these bands might extend many millimetres or centimetres in length whereas their thickness may be less than a few tens of microns. Moreover, the highly strained material within the ASB will continue to preserve a full physical continuity from one side to the other.

The ASB phenomenon in cold-headed parts is mainly a thermo-mechanically controlled phenomenon. It commonly occurs by impact loading at high strain rates and high strains. At the early stages of deformation, the work hardening mechanism dominates over the thermal softening mechanism causing an increase in the flow stress. On the other hand, 90–

ISSN (Online) 2456-1290

International Journal of Engineering Research in Mechanical and Civil Engineering (IJERMCE)

Vol 10, Issue 10, October 2023

95% of the plastic work is converted into heat leading to a local temperature increase and a flow stress decrease. Thus, a competing mechanism between the work hardening and thermal softening starts and continues in the deformation zone [8]. If the material deformation continues long enough, the thermal softening mechanism dominates over the work hardening mechanism which triggers unstable deformation. Nabil Basim [8] reported that this instability will force the deformation to localize into a narrower band. As a result, plastic deformation leads to a self-sustaining cycle of instability: Inhomogeneous plastic shear flow – non-uniform temperature distribution – local thermal softening and further inhomogeneous shear plastic flow that results in a highly localized shear band.

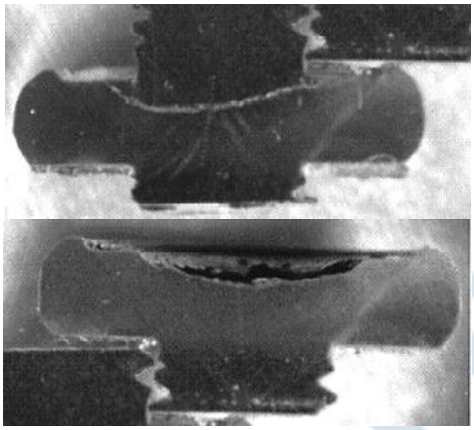

Fig.1 Failed cold-headed brass bolt along the ASB [9]

The situation in this stage is very critical as the material flow is unstable and strain localization takes place inside the band causing internal failure in cold-formed parts as shown in Fig. 1. Therefore, understanding the different stages of the ASB phenomenon, especially the instability phenomenon, is essential to have a better awareness about the failure mechanism in cold headed parts.

Marchand and Duffy [10] performed an intensive investigation of the initiation and propagation of ASBs in low alloy steel (HY-100) using the Kolsky bar torsion test and still cameras. This study proved that ASBs develop in three stages:

Stage I: The band will go through homogeneous plastic strain with an increase in flow stress.

Stage II: The second stage starts when the strain distribution becomes inhomogeneous. During this stage, the flow stress will continue to increase while the deformation proceeds accompanied by a decrease in the ASB width. A sudden drop in flow stress will mark the end of stage II and the beginning of stage III of ASB development.

Stage III: The sudden drop in flow stress triggered by the instability phenomenon is accompanied by an increase in nominal strains and a decrease in ASB width. The situation in this stage is very critical as the material flow is unstable and strain localization takes place inside the band.

1.2 Instability Criterion

Marchand and Duffy [10] reported that the instability stage (Stage III) of ASB development begins when the shear stress drops to approximately (95%) of its maximum value. Batra and Kim [11] and Batra and Lear [12] considered this value to be 90%, while Deltort [13] indicated that this value is 80%.

The work of Schoenfeld and Wright [14], Raftenberg [15], and Semiatin and Lahoti [16] employed the strain at the start of the instability stage in ASB development to quantify the following failure strain. Schoenfeld and Wright [14] derived a model that uses the homogeneous material response to anticipate the correct timing beyond the maximum stress at which stress collapse should occur.

Raftenberg [15] developed his failure criterion based on the amount of additional strain beyond the onset of instability. This was left as a parameter to be determined via experimental Hopkinson bar tests. He assumed that the effect of the strain rate change on instability is negligible since he assumed that the strain rate is constant.

Chen and Batra [17] based their material instability criterion on the delay between the ASB initiation and the instability stage. They found that the delay between the initiation of a shear band and the onset of material instability depends on the thermal-softening and strain and strain-rate hardening characteristics of the material, the loading conditions, and the shapes, sizes and number of defects present in the body. The instability stage (stage III) of ASB development usually leads shortly to an eventual ductile failure.

There is no doubt that the onset of instability or strain localization within the ASBs, followed by the stress collapse, is a very important factor in the development of ASB stages as it accelerates the deformation, leading to a fast ductile failure.

II. METHODOLOGY

The methodology to determine the material parameters for the workability criterion employs several steps presented in Fig. 2. These steps consist mainly of the drop weight compression test (DWCT) to simulate the CHP in conjunction with FE analysis implemented within ABAQUS/Explicit.

Metallographic inspection for the deformed specimens is performed to locate the failed zones inside the ASB. The experimental and FE simulation results are used to find the material constants for the new criterion. The failure measure in this work is taken to be the appearance of internal cracks along the ASB that exceed 100 μm in length.

A. Testing Materials

The CH quality AISI steel grades chosen for this research are 1018 steel and 1038 steel which represent low and medium carbon content steels. These materials were received in rod form from Ivaco Rolling Mills (Ontario, Canada).

ISSN (Online) 2456-1290

International Journal of Engineering Research in Mechanical and Civil Engineering (IJERMCE)

Vol 10, Issue 10, October 2023

Table 1 presents the chemical composition of the two steels under study. In general, the microstructure of the as-received 1018 steel and 1038 steel has similar grain size as shown in Fig. 3. Both microstructures consist of ferrite matrix and lamellar pearlite. However, the content of the ferrite and lamellar pearlite are different in the two microstructures due to the different carbon content. The microstructure study of 1018 steel reveals that the content of the lamellar pearlite and ferrite is around 25% and 75% respectively. Since the carbon content is the 1038 steel is higher; the microstructure of 1038 steel consists of 50% ferrite matrix and 50% lamellar pearlite.

Table1: Chemical Composition of the testing material (wt%)

AISI Steel grade	C	Mn	P	S	Si	Cu	Ni	Cr
1018	0.16	0.69	0.006	0.006	0.22	0.04	0.08	0.08
1038	0.38	0.82	0.007	0.002	0.19	0.04	0.08	0.08
AISI Steel grade	Mo	Sn	Al	N	B	V	Co	
1018	0.001	0.002	0.002	0.0026	0.0001	0.005	-	
1038	0.001	0.003	0.003	0.0044	0.0001	0.005	-	

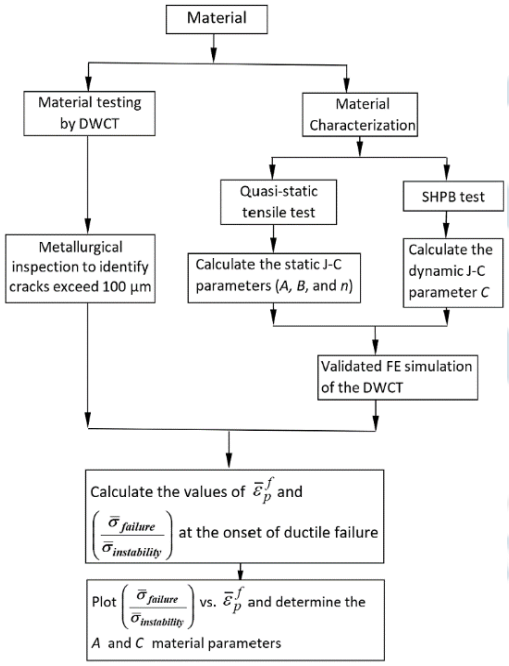

Fig. 2 The methodology used to determine the material parameters for the stress instability criterion.

2.2 Drop Weight Compression Test (DWCT

B. Drop Weight Compression Test (DWCT)

The DWCT as described by Nickoletopoulos [18] was used as a workability test to perform the cold heading of the specimens (Fig. 4). The DWCT facilitates the testing of the CHP and it is capable of generating internal cracks during upset testing. The DWCT machine (Fig. 4-a) consists of a tower enabling interchangeable weight plates to be dropped from heights up to 2.4 m. The die set configuration (Fig. 4-b) rests on a central column that is welded to the base of the DWCT machine. Specimens for CH were machined with a tolerance of 0.02 mm from as-rolled rod material to a cylindrical configuration of 5.3 mm in diameter with aspect ratios of 1.6 and 1.8. A series of tests is performed by varying the weights until the internal fracture is determined.

C. FE Simulation and Constitutive Model

The FE model implemented with ABAQUS/Explicit has been used to simulate the DWCT for the current work. The Johnson-Cook model (J-C) [19] is used to describe the thermo-plastic, rate-dependent behaviour of the material in a two-dimensional, axisymmetric, adiabatic, analysis of a cylindrical specimen under impact loading. The meshing of the specimen is performed using 4-noded continuum elements with reduced integration and hourglass control (CAX4R).

Accurate ASB modelling under high strain rate deformation processes over a wide range of strain rates and temperature changes requires reliable constitutive modelling of the stress–strain behaviour. This enables the prediction of flow stress collapse at the onset of the instability phenomenon during ASB development. The concept of stress collapse in adiabatic shear bands has been discussed in detail by Wright and Walter [20] who concluded that the stress drop and the onset of the instability phenomenon during high strain rate deformation is of greater importance than the localization of deformation.

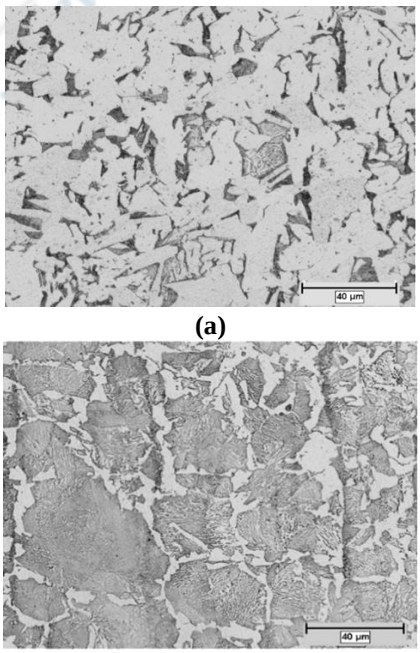

(a)

(b)

Fig. 3 As-received testing materials microstructure: (a) 1018 steel, (b) 1038 steel

The Johnson-Cook [19] model is used in the FE simulations of the current work because it provides a reasonably good prediction for high-rate deformation mechanical behaviour. This model is utilized extensively for

ISSN (Online) 2456-1290

International Journal of Engineering Research in Mechanical and Civil Engineering (IJERMCE)

Vol 10, Issue 10, October 2023

computational purposes because it also contains parameters that are relatively easy to determine. The J-C model has been successful in modelling the ASB phenomenon (see the works of Meyers et al. [21]; Johnson and Holmquist [22]; and Li and Jones [23]. This success is related to the model's ability to correctly predict the onset of strain instability marked by flow stress collapse during ASB development.

In the Johnson-Cook model, the Von-Mises flow stress is represented by a multiplicative relation as follows:

$$\bar{\sigma} = (A + B\bar{\varepsilon}_p{}^n)(1 + C\, ln\frac{\dot{\bar{\varepsilon}}_p}{\dot{\bar{\varepsilon}}_o})(1 - T*^m) \qquad (1)$$

Where $\bar{\sigma}, \bar{\varepsilon}_p$ and $\dot{\bar{\varepsilon}}_p$ are the effective flow stress, the effective plastic strain, and the effective plastic strain rate respectively. $\dot{\bar{\varepsilon}}_o$ is normally taken to be 1.0 s^{-1}. *A, B, n, C,* and *m* are material constants and *T** is the normalized temperature. The first term characterizes the strain hardening, whilst the second part accounts for strain rate dependence, and the last term captures the temperature effects.

D. Finding Johnson-Cook Parameters

The Split Hopkinson Pressure Bar (SHPB) is used to determine material response when subjected to deformation at high strain rates. Developed by Kolsky [24], the SHPB test has subsequently been used as a dependable method for determining the material behaviour at high strain rates that cannot be reached by traditional equipment such as hydraulic or screw-driven testing machines. Several SHPB tests were conducted on 5x5 mm cylinders to determine the dynamic J-C parameter (C).

Table 2. The final J-C parameters for both testing materials.

	Quasi-static parameters			Dynamic parameters	
Material	***A* (MPa)**	***B* (MPa)**	***n***	***C***	***m***
1018 steel	300	1000	0.76	0.05	1
1038 steel	420	1528	0.44	0.08	1

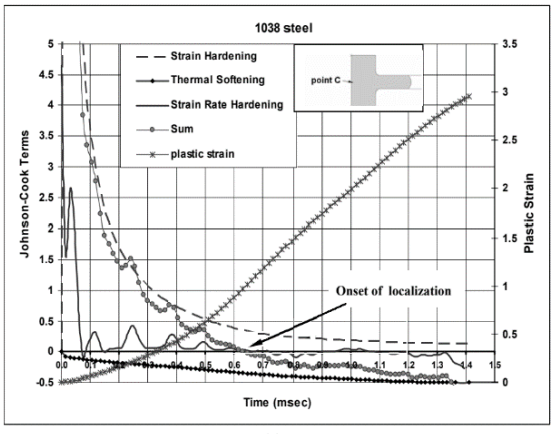

(a)

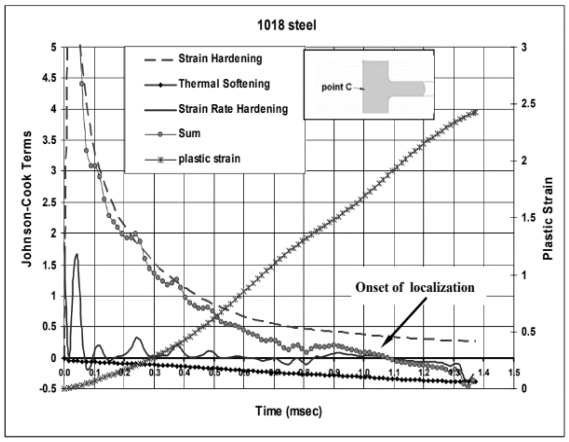

(b)

Fig. 5 Evolution of hardening and softening terms, indicating the onset of localization at the center of the DWCT specimen at point C: (a) 1038 steel and (b) 1018 steel.

On the other hand, the quasi-static tensile tests were performed on standard specimens to determine the J-C static parameters (A, B and n). The thermal softening constant, m, was set at 1, which has been reported to be a good approximation for several metals [19].

On the other hand, the quasi-static tensile tests were performed on standard specimens to determine the J-C static parameters (A, B and n). The thermal softening constant, m, was set at 1, which has been reported to be a good approximation for several metals [19].

This onset of localization occurs when an increase in the equivalent plastic strain results in a decrease in the equivalent stress. This can be indicated by the maximum value of the equivalent stress-equivalent plastic strain relation. This can be expressed as:

$$\frac{d\bar{\sigma}}{d\bar{\varepsilon}_p} \leq 0 \qquad (2)$$

Taking the equivalent stress to be a function of equivalent plastic strain, the equivalent strain rate, and temperature, Equation 2 may be written as:

By applying this to the J-C model utilized in this work the following is obtained:

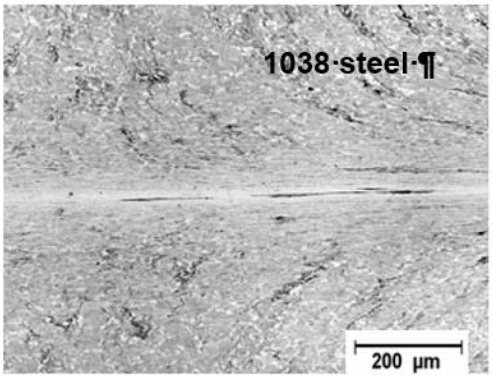

(a)

ISSN (Online) 2456-1290

International Journal of Engineering Research in Mechanical and Civil Engineering (IJERMCE)

Vol 10, Issue 10, October 2023

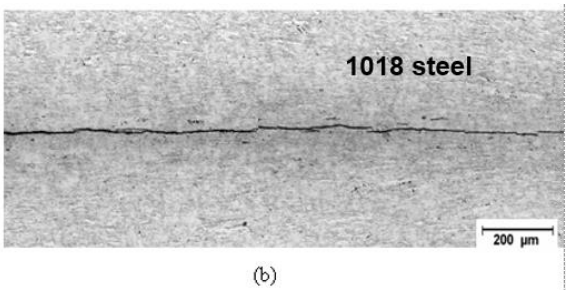

(b)

Fig. 6. Elongated cracks along a localized ASB in (a) 1038 steel (aspect ratio= 1.8, drop height= 2.4 m, drop weight= 30.5 kg) (etchant: 2% Nital solution) (b) 1018 steel (aspect ratio= 1.8, drop height= 2.4 m, drop weight= 37.6 kg)

$$\frac{Bn(\bar{\varepsilon}_p)^{n-1}}{A+B(\bar{\varepsilon}_p)^n} + \frac{C/\dot{\bar{\varepsilon}}_p}{1+C\ ln\frac{\dot{\bar{\varepsilon}}_p}{\dot{\bar{\varepsilon}}_o}} \frac{d\dot{\bar{\varepsilon}}_p/dt}{d\bar{\varepsilon}_p/dt} + \frac{-mT^{*m-1}}{(1-T^{*m})(T_m-T_o)} \frac{dT/dt}{d\bar{\varepsilon}_p/dt} \leq 0 \quad (3)$$

The first and second terms in this expression represent the strain hardening and the strain rate-hardening effect, respectively, while the third term represents the thermal softening effect. Equation 3 gives the conditions for the onset of instability and strain localization. One way to determine this is by using Equation 3, from which the strain hardening term, rate hardening term, and thermal softening terms are plotted at a location within the region of maximum strain. Here, all the required data were collected from the FE simulation results.

Fig. 5 indicates that the sum of the three terms becomes negative at an approximate equivalent plastic strain of 0.97 and 1.9 for the 1038 steel and 1018 steel DWCT specimens, respectively.

III. RESULTS AND DISCUSSION

In general, microscopic and metallurgical examination of the DWCT specimens at different levels of deformation showed that voids and cracks that exceed 100 µm were found along the ASBs inside DWCT specimens (Fig. 6).

Finite element simulation runs were performed for the DWCT tests taking into account the different dropped weights used. Simulation results were used to study the changes in flow stress and equivalent plastic strain at different locations of the specimens. The sample of the finite element simulation results of the equivalent plastic strain and equivalent flow stress contours for a DWCT specimen are shown in Fig. 7.

The material constants of the ductile fracture criterion

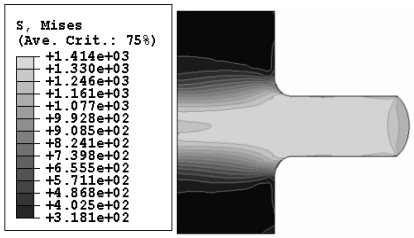

Equivalent stress

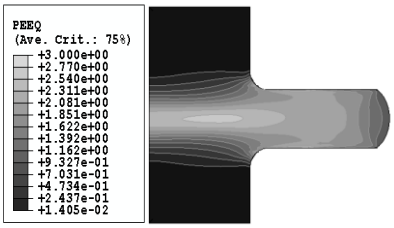

Equivalent plastic strain

Fig. 7 Finite element contours: (a) equivalent plastic strain; and (b) Equivalent flow stress

were determined in several steps by combining the results of the metallographic inspection and the FE simulation runs for the series of DWCTs. The first step is to indicate the position of each internal or external crack that exceeds 100 µm in length. Using the FE simulation contours for each DWCT specimen, the elements that correspond to the failed locations on the DWCT specimen were indicated. This was followed by determining the time the equivalent stresses, the equivalent plastic strain at the onset of instability and the crack growth to 100 µm in length and more for these elements are to be used in finding the material parameters for the criterion.

For these failed locations, the $\bar{\varepsilon}_p^f$ and the ratio $\left(\frac{\bar{\sigma}_{failure}}{\bar{\sigma}_{instability}}\right)$ values were calculated from the FE simulations of the corresponding specimens.

The relationship between $\left(\frac{\bar{\sigma}_{failure}}{\bar{\sigma}_{instability}}\right)$ and $\bar{\varepsilon}_p^f$ was plotted for all failed locations to calculate the material constants *A* and *C*

$$\bar{\varepsilon}_p^f = C + A\left(\frac{\bar{\sigma}_{failure}}{\bar{\sigma}_{instability}}\right) \quad (4)$$

To set the final workability limit, the trend passing through the plotted points is lowered vertically to keep all the failure points above it. This final workability limit acts as a lower boundary separating the failure zone from the no-failure zone which can be used in the CH design and optimization processes. The slope of this linear relationship is given by the *A* parameter while the material constant *C* is the intersection of the ordinate and this line. This final workability limit acts as a lower boundary separating the failure zone from the no-failure zone and can be used in CH design and optimization processes. The final workability limits of the stress instability workability criterion of 1018 steel and 1038 steel are shown in Fig. 8.

These workability limits separate the fail-no-fail zones and can be used in optimizing the multistage die design of the CH process. If the relationship between $\left(\frac{\bar{\sigma}_{failure}}{\bar{\sigma}_{instability}}\right)$ and $\bar{\varepsilon}_p^f$

ISSN (Online) 2456-1290

International Journal of Engineering Research in Mechanical and Civil Engineering (IJERMCE)

Vol 10, Issue 10, October 2023

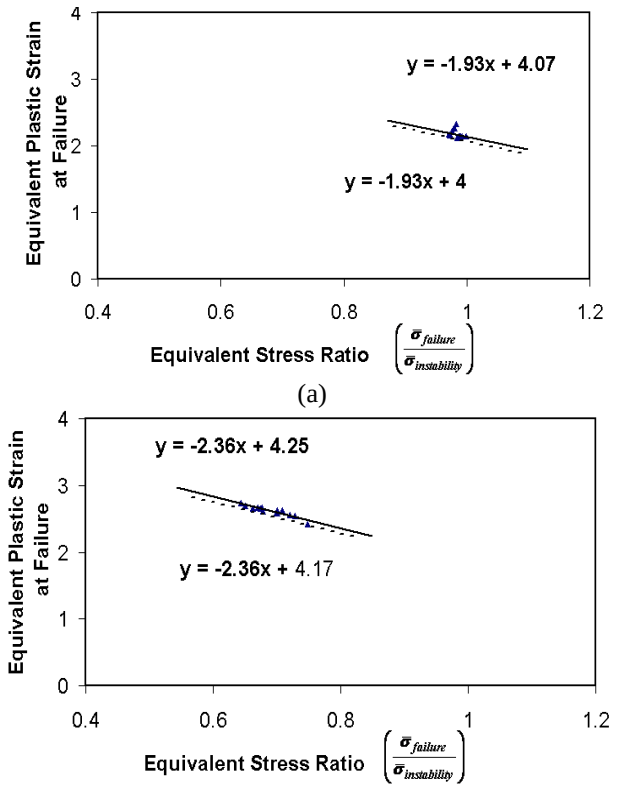

Fig. 8 The workability limits of the internal ductile failure in the CH process using the stress instability criterion: (a) 1018 steel, (b) 1038 steel.

The solid line is the trend line of all failed points and the broken line presents the safe workability limits.

within the highly deformed zones always below the workability limits, then deformed material will not reach the stress instability stage. Hence, the multistage die design under study will result in defect-free CH parts.

IV. CONCLUSIONS

A new technique to set a new workability criterion for predicting the limits for internal ductile failure in cold-headed steel parts is presented with a comprehensive experimental and finite element simulation methodology. This methodology consists of the DWCT to simulate the CHP, Hopkinson bar test in conjunction with metallographic inspection and finite element analyses (implemented within ABAQUS/Explicit) and has been applied to determine the workability limits for 1018 and 1038 steels in CHP. The new workability criterion is based on using the ratio between the equivalent stress at instability and failure as an indicator to accurately reveal the locus of initiation of internal ductile failures.

The workability limits introduced in the new ductile failure workability criterion can be integrated into the finite element simulation models to be utilized as an efficient tool in optimizing the die design of the multistage cold heading process.

REFERENCES

[1] C A. Sabih, J.A. Nemes, “Internal ductile failure mechanisms in steel cold heading process”, Journal of Materials Processing Technology, vol. 209, Issue 9, pp. 4292-4311, 2009.

[2] R.J., Clifton, “ Adiabatic shear banding. In Material Response to Ultra-High Loading Rates NMAB-356. National Materials Advisory Board (NRC). Washington DC. Ch. 8, pp. 129-142, 1980.

[3] Y.L. Bai, “Thermo-plastic instability in simple shear”, Journal of the Mechanics and Physics of Solids, vol. 30, Issue 4, pp. 195-207, 1982.

[4] A.M. Merzer, “Modelling of adiabatic shear band development from small imperfections”, Journal of the Mechanics and Physics of Solids, vol. 30, Issue 5, pp. 323-338, 1982.

[5] T.W. Wright, and R.C. Batra, “The initiation and growth of adiabatic shear bands”, International Journal of Plasticity, vol. 1, Issue 3, pp. 205-212,1985.

[6] M.A. Meyers, and C.L. Wittman, "Effect of Metallurgical Parameters on Shear Band Formation in Low-Carbon (~0.20 wt. pct.) Steels", Metallurgical Transaction A, vol. 21A, pp. 3153-3164, 1990.

[7] J.R. Klepaczko, and B. Rezaig, “A numerical study of adiabatic shear banding in mild steel by dislocation mechanics based constitutive relations”, Mechanics of Materials, vol. 24, Issue 2, pp. 125-139, 1996.

[8] M. Nabil Bassim, “Study of the formation of adiabatic shear bands in steels”, Journal of Materials Processing Technology, vol. 119, Issues 1–3, pp. 234-236, 2001.

[9] W. Reitz, “Failure analysis of brass bolt from mausoleum”, Journal of Failure Analysis and Prevention, vol. 5, pp. 20-25, 2005.

[10] Marchand, and J. Duffy, “An experimental study of the formation process of adiabatic shear bands in a structural steel”, Journal of the Mechanics and Physics of Solids, vol. 36, Issue 3, pp. 251-283, 1988.

[11] R.C. Batra, and N.M. Wilson, “Adiabatic shear bands in plane strain deformations of a WHA”, International Journal of Plasticity, vol. 14, Issues 1–3, pp. 43-60, 1998.

[12] R.C. Batra, and M.H. Lear, “Adiabatic shear banding in plane strain tensile deformations of 11 thermoelastoviscoplastic materials with finite thermal wave speed”, International Journal of Plasticity, vol. 21, Issue 8, pp. 1521-1545, 2005.

[13] Deltort, “Experimental and numerical aspects of adiabatic shear in a 4340 steel”, Journal de Physique IV, France Colloq. vol. 4, pp. 447–452, 1994.

[14] S.E. Schoenfeld, and T.W. Wright, “A failure criterion based on material instability”, International Journal of Solids and Structures, vol. 40, Issue 12, pp. 3021-3037, 2003.

[15] M.N., Raftenberg, “A shear banding model for penetration calculations”, International Journal of Impact Engineering, vol. 25, pp. 123–146, 2001.

[16] S.L. Semiatin, G.D Lahoti, an S.I Oh, “The Occurrence of Shear Bands in Metalworking”, In: Mescall, J., Weiss, V. (eds) Material Behavior Under High Stress and Ultrahigh Loading Rates. Sagamore Army Materials Research Conference Proceedings, vol. 29. pp. 119-159, 1983.

[17] L. Chen, and R.C Batra, “Material instability criterion near a notch-tip under locally adiabatic deformations of thermoviscoplastic materials”, Theoretical and Applied

Fracture Mechanics, vol. 30, Issue 2, pp. 153-158,1998.

[18] N. Nickoletopoulos," Physical and numerical modeling of fracture during Upsetting for Cold Heading Operations", Doctoral dissertation, McGill University at Montreal, 2000

[19] G. R. Johnson, and W. H. Cook, "A constitutive model and data for metals subjected to large strains, high strain rates and high temperatures," In Proceedings of the Seventh International Symposium on Ballistic, pp. 541-547. The Hague, Netherland, 1983.

[20] T.W. Wright, and J.W. Walter, "On stress collapse in adiabatic shear bands", Journal of the Mechanics and Physics of Solids, vol. 35, Issue 6, pp. 701-720, 1987.

[21] M.A. Meyers, G. Subhash, B.K. Kad, and L. Prasad, "Evolution of microstructure and shear-band formation in α-hcp titanium", Mechanics of Materials, vol .17, Issues 2–3, pp. 175-193, 1994

[22] G.R. Johnson, and T.J. Holmquist, "Evaluation of cylinder-impact test data for constitutive model constants", Journal of Applied Physics, vol. 64, Issue 8, pp 3901 – 3910, 1988.

[23] Q.M. Li, N. Jones," Response and failure of a double-shear beam subjected to mass impact", International Journal of Solids and Structures, vol. 39, Issue 7, pp. 1919-1947, 2002.

[24] H. Kolsky, "An investigation of the mechanical properties of materials at very high rates of loading," In Proceeding of the Physical Society, section B., vol. 62, pp. 676-700, 1949.